Parametric resonances in a photonic time crystal with periodic square modulation of its permittivity $\varepsilon(t)$

J. L. Valdez-García [*] and P. Halevi [†]
Instituto Nacional de Astrofísica, Óptica y Electrónica, Tonantzintla, 72840 Puebla, México

(Received 12 July 2023; accepted 27 March 2024; published 18 June 2024)

We study parametric resonances in a "temporal photonic crystal" or "photonic time crystal" (PTC) slab whose permittivity is assumed to be modulated periodically in time in a stepwise manner (with abrupt transitions). These resonances in the light reflected and transmitted by the PTC slab occur when the modulation frequency assumes a series of eigenvalues that are inversely proportional to the slab thickness, in addition to having a value that is twice that of the frequency of incidence. We compare the reflection and transmission spectra with those for a harmonically modulated slab and find marked, qualitative differences. These depend crucially on the modulation strength and on the impedance contrast at the slab's interfaces. In the special case of weak modulation, the differences in behavior between the two forms of modulation can be traced to a simple scaling factor. In principle, these findings could be corroborated with infrared light incident on PTC slabs tens of micrometers thick.

DOI: 10.1103/PhysRevA.109.063517

I. INTRODUCTION

This paper concerns optical modes in dynamic media, namely, media whose properties such as permittivity and/or permeability vary with time. A book [1] and a very recent review [2] are devoted to this emerging field, so our references will be restricted mostly to those that are essential to the present work. Singling out a few very recent publications, we note that dispersion and absorption have been incorporated into the study of refraction at a temporal discontinuity, leading to the conclusion that two additional boundary conditions are required [3]. Time modulation can also affect thermal behavior: reciprocal thermal diffusion was experimentally demonstrated in such dynamic media [4] and it was also shown that near-field thermal radiation can be coherently controlled [5].

Here, we deal with "temporal photonic crystals" or "photonic time crystals" (PTCs); the word "crystal" suggesting periodicity. Specifically, we are assuming that the permittivity is a periodic function of time [6,7]. The study of optical modes in such media has taken great impetus with the realization of an Al-doped zinc oxide film that was pumped at infrared frequencies [8] and by simulations of excitations by means of dipole or atomic emission [9] and free electron motion [10].

In the case of ordinary (spatially periodic) photonic crystals propagation is allowed in certain frequency bands that are separated by frequency gaps. In PTCs, to the contrary, any value of the frequency is permitted and a band structure of wave number bands, separated by wave number gaps, is obtained [6,7,9]. The first observation of such a gap was reported in the microwave regime for a transmission line [11,12]. Direct incidence of monochromatic light should excite an infinite number of plane waves (with different wave lengths) of the same frequency, as well as harmonics of this frequency, a consequence of Floquet's theorem. On the other hand, a wave number within a band gap can be excited only by special methods [9,10] and this results in growth of the wave amplitude, namely, instabilities.

The above comments pertain to bulk modes of the PTC. Boundaries can affect the outcome in important ways. A PTC with modulation of the permittivity can lead to parametric resonances (PRs) [6,13], as is also the case for modulation of the permeability or simultaneous modulation of both permittivity and permeability [14]. Such resonances give rise to huge amplifications of the fields that are reflected and transmitted by the slab; this can be attained for a series of values of the frequency of modulation (for a given slab thickness) or for special thicknesses (while keeping constant the modulation frequency). Very recently it was pointed out that, strictly at resonance, Floquet's theorem requires an amendment [15] and that this should lead to linear growth in time of the light reflected from a slab on a metallic substrate [16]. Parametric Mie resonances in modulated scatterers were also reported [17].

Most work in this field assumes harmonic modulation in time. Recently, however, we have been exploring square modulation (with abrupt alternations of the permittivity and/or permeability in time) as well. We found that the behavior strongly differs depending on whether the permittivity and permeability oscillate in phase or out of phase [18], and surprisingly, the band structure and the growth pattern (for the wave number within a forbidden band) can be periodic in the wave number itself, in addition to the usual periodicity in frequency [19]. Here we continue this line of investigation, exploring the PRs in a PTC with the square profile of its permittivity. In our calculations of the eigenvalues (dispersion relation) and the reflection and transmission coefficients of the slab we closely follow the general theoretical treatments

[*] jlvaldez@inaoep.mx
[†] halevi@inaoep.mx

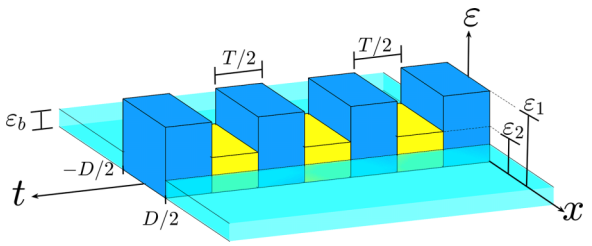

FIG. 1. The relative permittivity $\varepsilon_r(t)$ of a slab of thickness D is periodically modulated in time, alternating stepwise between the values ε_1 and ε_2 every half-period T. This dynamic slab is bounded by a medium of static relative permittivity ε_b.

of Ref. [7], while the theory of the parametric resonances is based on Ref. [14]. That said, despite the formal analogy, we find substantial qualitative and quantitative differences in behavior in comparison to the case of harmonic modulation [14].

Section II is devoted to the theoretical development of the PRs, including definition of the system (Sec. II A), the bulk eigenvalue problem (Sec. II B), the reflection and transmission coefficients for the dynamic slab (Sec. II C), the eigenvalue problem for the resonances (Sec. II D), and some simple formulas for the approximation of weak modulation (Sec. II E). The numerical results are presented and discussed in Sec. III, concluding the paper in Sec. IV.

II. THEORETICAL DEVELOPMENT OF THE PARAMETRIC RESONANCES

A. Definition of the system

As can be seen in Fig. 1, the relative permittivity $\varepsilon_r(x,t)$ of our system depends both on the spatial coordinate x and on the time t. Namely, the PTC occupies the space between $x=-D/2$ and $x=D/2$, with its relative permittivity switching from ε_1 to ε_2 and back to ε_1 every $T/2$ seconds. This slab of thickness D is bounded (for $x<-D/2$ and $x>D/2$) by a medium of constant relative permittivity ε_b. The relative permeabilities are also assumed to be constant, μ_r for the slab and μ_b for the bounding medium. In brief, Fig. 1 describes a PTC slab, with its permittivity modulated abruptly at the circular frequency $\Omega=2\pi/T$, embedded in a static medium.

For a more realistic description of the PRs we also allow for some absorption within the slab, characterized by a constant imaginary part of the relative permittivity, ε_r''. Then we can express the relative permittivity within a single period in terms of the modulation strength (or, briefly, modulation) m_ε as

$$\varepsilon_r(t)=\begin{cases}\varepsilon_1=\bar{\varepsilon}_r(1+m_\varepsilon)+i\bar{\varepsilon}_r'', & 0<t<T/2,\\ \varepsilon_2=\bar{\varepsilon}_r(1-m_\varepsilon)+i\bar{\varepsilon}_r'', & T/2<t<T.\end{cases} \tag{1}$$

Here, $\bar{\varepsilon}_r$ is the simple average of ε_1 and ε_2 or $m_\varepsilon=(\varepsilon_1-\varepsilon_2)/(2\bar{\varepsilon}_r)$.

B. Bulk eigenvalue problem

First we consider a plane wave of wave number k propagating in the bulk PTC. As in Refs. [6,7], in such a dynamic medium the electric field $E(t)e^{ikx}$ satisfies the wave equation

$$\frac{d^2}{dt^2}[\mu_r\varepsilon_r(t)E(t)]+k^2c^2E(t)=0, \tag{2}$$

with c being the vacuum speed of light. Then expanding $\varepsilon_r(t)$ in a Fourier series, the Floquet theorem leads to the following eigenvalue equation for the eigenvectors e_{pn}:

$$\sum_n\left[\hat{\varepsilon}_{m-n}(\hat{\omega}-m)^2-\hat{k}_p^2\delta_{mn}\right]e_{pn}(\hat{\omega})=0. \tag{3}$$

Here, $p=1,2,\ldots,$ are the serial indexes of the first, second, and so on wave number bands and $m,n=0,\pm1,\pm2,\ldots,$ are the indexes of the time-harmonics created by the modulation. ε_{m-n} are the Fourier coefficients of $\varepsilon_r(t)$ and δ_{mn} is the Kronecker delta. For convenience we normalized the wave number k and the frequency ω as follows:

$$\hat{k}_p=\frac{k_pc}{\Omega\sqrt{\mu_r\bar{\varepsilon}_r}}, \tag{4}$$

$$\hat{\omega}=\frac{\omega}{\Omega}. \tag{5}$$

For every value of the band index p, Eq. (3) represents an infinite number of equations in the index m for the infinite number of unknowns e_{pn}. Equating to zero the determinant of the coefficients of e_{pn} relates $\hat{\omega}$ and $\hat{k}$ and thus leads to the dispersion relation for the optical modes of our time-periodic medium.

C. Reflection and transmission coefficients

The electric-field amplitudes within the PTC slab, A_p and B_p, and the reflection and transmission coefficients r_n and t_n were originally calculated in Ref. [7] and in a generalized form (to take into account a possible change of impedance at the slab interfaces) in Ref. [20]. They were obtained by imposing the conditions that the electric and magnetic fields $E(t)$ and $H(t)$ must be continuous at both slab interfaces at every instant of time. The amplitudes A_p and B_p are obtained from the following coupled set of equations:

$$\sum_p\left[e_{pn}+\sum_m\frac{\hat{\varepsilon}_{n-m}(\hat{\omega}-n)\hat{Z}}{\hat{k}_p}e_{pm}\right]\frac{A_p}{E_0}+\sum_p\left[e_{pn}-\sum_m\frac{\hat{\varepsilon}_{n-m}(\hat{\omega}-n)\hat{Z}}{\hat{k}_p}e_{pm}\right]\frac{B_p}{E_0}=2\delta_{n0}, \tag{6}$$

$$\sum_p\left[e_{pn}-\sum_m\frac{\hat{\varepsilon}_{n-m}(\hat{\omega}-n)\hat{Z}}{\hat{k}_p}e_{pm}\right]\frac{A_p}{E_0}e^{i\hat{k}_p\nu}+\sum_p\left[e_{pn}+\sum_m\frac{\hat{\varepsilon}_{n-m}(\hat{\omega}-n)\hat{Z}}{\hat{k}_p}e_{pm}\right]\frac{B_p}{E_0}e^{-i\hat{k}_p\nu}=0. \tag{7}$$

The calculation of A_p and B_p requires that the bulk eigenvalue problem be first solved. Namely, e_{pn} and $\hat{\omega}(\hat{k})$ from Eq. (3) have to be substituted in the Eqs. (6) and (7). The relative impedance $\hat{Z}$ is defined as

$$\hat{Z}=\frac{\sqrt{\mu_r/\bar{\varepsilon}_r}}{\sqrt{\mu_b/\varepsilon_b}}. \tag{8}$$

Also, the normalization process leads to the important parameter ν, defined as

$$\nu = \frac{D\Omega\sqrt{\mu_r\bar{\varepsilon}_r}}{c}. \tag{9}$$

Finally, the reflection and transmission coefficients are found from the following equations:

$$r_n = \sum_p \left(\frac{A_p}{E_0} + \frac{B_p}{E_0}\right) e_{pn} - \delta_{n0}, \tag{10}$$

$$t_n = \sum_p \left(\frac{A_p}{E_0} e^{i\hat{k}_p\nu} + \frac{B_p}{E_0} e^{-i\hat{k}_p\nu}\right) e_{pn}. \tag{11}$$

D. Eigenvalue problem for the resonances

Here, we pose the central question of the issue at hand: Is the PTC slab capable of self-sustained oscillations of optical fields? If the answer were affirmative, then Maxwell's Equations would have legitimate solutions inside and outside the PTC slab even with the imposition of $E_0 = 0$, namely, no field incident on the slab. We could proceed by multiplying Eqs. (6) and (7) by E_0, followed by the substitution $E_0 = 0$; however, it is more instructive to take advantage of the simple spatial symmetry that implies that the fields $E(t)$ be either symmetric or antisymmetric. This approach was followed in Ref. [14] for the more general situation of modulation in time of both the permittivity and the permeability. In the present case of interest, that $\mu(t)$ is constant, we obtain that

$$\sum_p \left\{\hat{Z}(\hat{\omega} - n) f\left(\frac{\hat{k}_p\nu}{2}\right) + i\hat{k}_p f'\left(\frac{\hat{k}_p\nu}{2}\right)\right\} e_{pn}E_p = 0, \tag{12}$$

$$f(\hat{k}_p\nu) = \begin{cases} \cos(\hat{k}_p\nu) & \text{for the symmetric modes,} \\ \sin(\hat{k}_p\nu) & \text{for the antisymmetric modes.} \end{cases} \tag{13}$$

Equation (12) is an additional eigenvalue equation; although its solution necessitates the prior solution of the bulk eigenvalue problem, Eq. (3), it determines the conditions for self-sustained or natural modes of the PTC plate. The band amplitudes E_p are the eigenvectors, determining the specific field profile of the electric field in the slab. Equation (12) is expected to have solutions only for special values of the parameter ν; these are the eigenvalues. In practical terms this means that, for a PTC slab of given thickness D there should exist self-sustained oscillations only for certain modulation frequencies Ω. The opposite is true if Ω is specified, normal modes can exist only for special values of D. The dimensionless parameter ν thus concisely expresses both the D values (for given Ω) and the Ω values (for given D) for which parametric resonances are possible.

E. Weak modulation approximation

This approximation is based on the assumption that $m_\varepsilon \ll 1$ in Eq. (1), meaning that $(\varepsilon_1 - \varepsilon_2) \ll (\varepsilon_1 + \varepsilon_2)$ in Fig. 1. In this situation, presumably, only the first two harmonics ($n = 0$ and $n = 1$) and the first two bands ($p = 1$ and $p = 2$) are appreciably excited. The approximation has turned out surprisingly good even for modulations as high as $m_\varepsilon = 0.5$ [20,14]. Also, it is well known that parametric resonances are strongest when the modulation frequency is twice as great as the natural frequency of oscillation, so in this subsection we assume that $\omega = \Omega/2$.

Under the above-noted assumptions Eq. (12) reduces to

$$\frac{\hat{Z}^2 - 1}{\hat{Z}^2 + 1}\cos\left(\frac{\nu}{2}\right) \pm \cos\left(\frac{\nu m_\varepsilon}{2\pi}\right) = 0. \tag{14}$$

The + and − signs here correspond, respectively, to symmetric and antisymmetric oscillations of the electric field in the slab. Changing the parameter $\hat{Z}$ to $1/\hat{Z}$ merely changes the sign of the first term of Eq. (14); hence, if a certain value of ν is an eigenvalue for a given value of $\hat{Z}$, this ν is still an eigenvalue for its reciprocal $1/\hat{Z}$, however, with a change of symmetry. Namely, a symmetric field for $\hat{Z}$ becomes antisymmetric for $1/\hat{Z}$ and vice versa. This property turns out to be valid even for modulations that are not small, as will be seen in the next section. Equation (14) has multiple solutions for the eigenvalue ν, these depend on the modulation m_ε and on the relative impedance $\hat{Z}$.

In the limit $m_\varepsilon \to 0$, Eq. (14) becomes

$$\cos\left(\frac{\nu}{2}\right) = \pm\left(\frac{\hat{Z}^2 + 1}{\hat{Z}^2 - 1}\right). \tag{15}$$

We note that Eqs. (14) and (15) are similar to the Eqs. (17) and (21) of Ref. [14]; however, Eq. (15) cannot be satisfied. This is hardly surprising since, in the absence of modulation (for a static slab) there are no parametric resonances. A more interesting limit of Eq. (14) is gotten for a PTC whose average impedance matches that of the bounding medium, $\hat{Z} = 1$:

$$\cos\left(\frac{\nu m_\varepsilon}{2\pi}\right) = 0. \tag{16}$$

Thus, the solutions are

$$\nu = \frac{\pi^2}{m_\varepsilon} s, \quad s = 1,\ 3,\ 5, \cdots. \tag{17}$$

Then the smallest value of ν that gives rise to resonance is π^2/m_ε. The corresponding formula for the case of harmonic modulation (see Eq. (20) of Ref. [14]) was found to be $\nu = 4\pi s/m_\varepsilon$, thus occasioning the lowest resonance at $\nu = 4\pi/m_\varepsilon$, a value about 27% greater than for the square modulation.

Another interesting special case obtains for $\hat{Z} \ll 1$ or for $\hat{Z} \gg 1$. According to the definition of $\hat{Z}$, Eq. (8), $\hat{Z} \ll 1$ describes the case of a geometry where the bounding medium of the slab is an "epsilon-near-zero" (ENZ) material, namely, $\varepsilon_b \ll \bar{\varepsilon}_r$. On the other hand, for $\hat{Z} \gg 1$, this inequality is reversed, $\bar{\varepsilon}_r \ll \varepsilon_b$, namely, it is the modulated dielectric that is the ENZ material. Taking the limits $\hat{Z} \to 0$ or $\hat{Z} \to \infty$, Eq. (14) reduces to

$$\cos\left(\frac{\nu}{2}\right) \pm \cos\left(\frac{\nu m_\varepsilon}{2\pi}\right) = 0. \tag{18}$$

Then simple algebra gives the solutions

$$\nu = 2\pi\left(1 \pm \frac{m_\varepsilon}{\pi}\right)s, \quad s = 1,\ 2,\ 3, \cdots. \tag{19}$$

Because $m_\varepsilon \ll 1$, these describe doublets that are centered at all the integral multiples of 2π. And these ν values are $\sim(1/m_\varepsilon)$ times smaller than those given by Eq. (17) for $\hat{Z} = 1$.

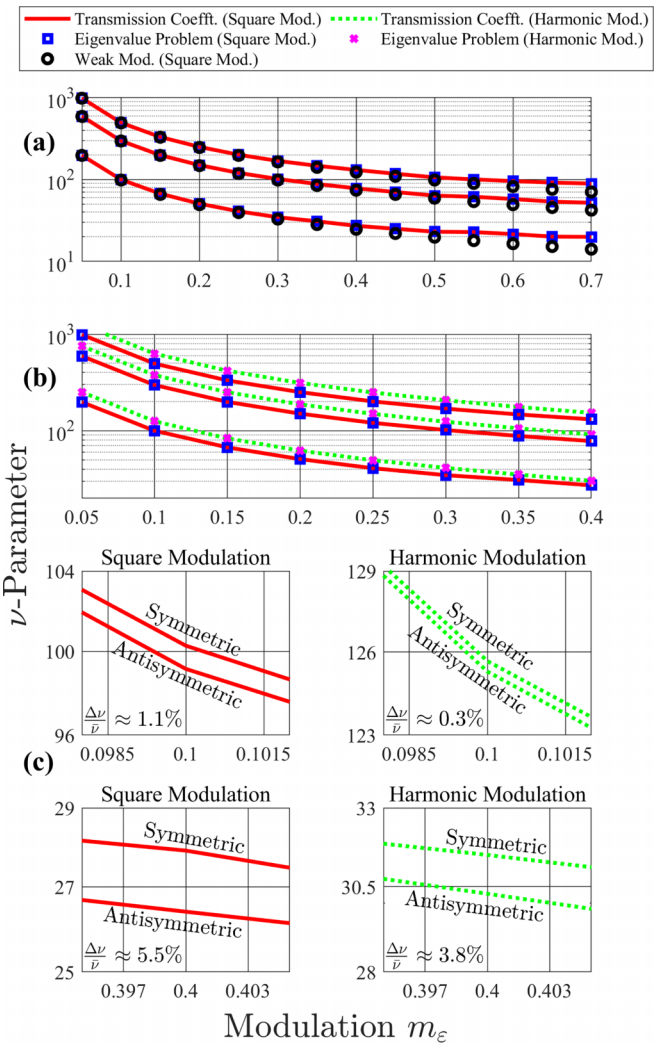

FIG. 2. (a) Three eigenvalues of the parameter ν for square modulation, defined in Eq. (9), as function of the modulation strength m_ε. We compare three different methods of calculation, based on the transmission coefficients Eq. (11), the eigenvalue equation Eq. (12), and the weak modulation approximation Eq. (17). Note the exact coincidence of the first two methods and good coincidence of the third method for $m_\varepsilon < 0.5$. (b) Comparison of eigenvalues of the ν parameter for square modulation and harmonic modulation, using the transmission coefficient method Eq. (11) and the eigenvalue equation Eq. (12). (c) Fine structure of the ν parameter for the square and harmonic modulations for $m_\varepsilon \cong 0.1$ and $m_\varepsilon \cong 0.4$. This splitting $\Delta\nu$, corresponding to symmetric and antisymmetric modes $E(x)$ in the slab, was unresolved in (a) and (b). It is assumed that $\hat{Z} = 1$, $\hat{\omega} = 1/2$, and $\varepsilon_r'' = 0$

How does this compare to the case of harmonic modulation? By inspection of Eq. (17) of Ref. [14] we can see that the only change is that, in Eqs. (18) and (19) we have to replace m_ε/π by $m_\varepsilon/4$, so that

$$\nu_{\text{harm}} = 2\pi\left(1 \pm \frac{m_\varepsilon}{4}\right)s, \qquad s = 1,\ 2,\ 3, \cdots . \tag{20}$$

Hence, the doublets are still positioned at integral multiples of 2π, however, their splitting is $(\pi m_\varepsilon)s$ for the harmonic modulation, while it is $(4m_\varepsilon)s$ for the square modulation.

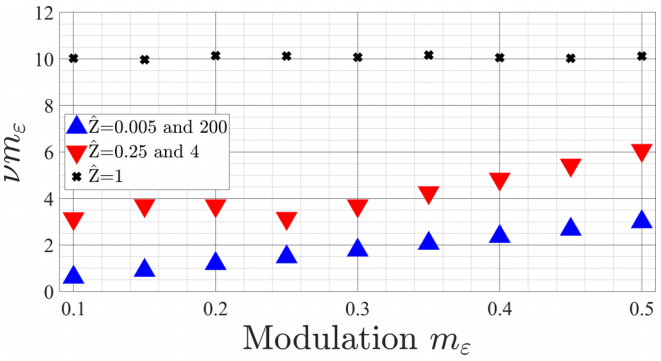

FIG. 3. The product νm_ε for the first eigenvalue of Eq. (12) as function of the modulation m_ε. Results are compared for five values of the relative impedance $\hat{Z}$, defined by Eq. (8). Here, $\hat{\omega} = 0.5$ and $\varepsilon_r'' = 0.0001$. Note that, for $\hat{Z} = 1$, $\nu m_\varepsilon = \pi^2$ [as given by the weak approximation formula (17)] even for strong modulations. All the resonances for $\hat{Z} = 0.005$ are antisymmetric and for $\hat{Z} = 200$ they are symmetric. In the case of $\hat{Z} = 0.25$ and $\hat{Z} = 4$ there are both symmetric and antisymmetric resonances. The symmetry of the resonances for $\hat{Z}$ is the opposite of the resonances for $1/\hat{Z}$. All these eigenvalues split [analogously to Fig. 2(c)], the amount of splitting depending on $\hat{Z}$

All the resonances for $m_\varepsilon \ll 1$ are associated with the intersection of two cosine functions in Eq. (14) (and Eq. (17) of Ref. [14]), one oscillating rapidly and the other slowly. This point, as well as the creation of the doublets, is vividly illustrated in Figs. 3(a) and 3(b) of Ref. [14].

Let's consider the implications for the average wavelength in the slab $\lambda_\Omega = 2\pi c/\Omega(\mu_r\bar{\varepsilon}_r)^{1/2}$, while maintaining the modulation frequency at the value $\Omega = 2\omega$ that gives rise to the strongest resonances. Then the definition of ν, Eq. (9), gives

$$\frac{D}{\lambda_\Omega/2} = \frac{\nu}{2\pi}. \tag{21}$$

The discussion being limited to weak modulation, $m_\varepsilon \ll 1$, in this subsection, if either the dynamic medium or the bounding media are ENZ materials, then Eqs. (19) and (20) give

$$\frac{D}{\lambda_\Omega/2} = \left\{\begin{matrix}(1 \pm m_\varepsilon/\pi)s \text{ for square mod.} \\ (1 \pm m_\varepsilon/4)s \text{ for harmonic mod.}\end{matrix}\right\}$$
$$\text{for } s = 1,\ 2,\ 3, \ldots, \hat{Z} \ll 1 \text{ or } \hat{Z} \gg 1. \tag{22}$$

This has the simple interpretation that parametric resonances are excited in the form of doublets whenever an integer number of half-wavelengths fits into the slab width. Thus, while these doublets appear at the wavelengths $\lambda_\Omega = 2D,\ 2D/2,\ 2D/3$, and so on for both the square and the harmonic modulations (and, likely, for any type of periodic modulation) the splittings $\delta\lambda_\Omega$ depend on the form of the modulation:

$$\frac{\delta\lambda_\Omega}{\lambda_\Omega} = \left\{\begin{matrix}(2/\pi)\, m_\varepsilon \text{ for square modulation} \\ (1/2)\, m_\varepsilon \text{ for harmonic modulation}\end{matrix}\right\}$$
$$\text{for } \hat{Z} \ll 1 \text{ or } \hat{Z} \gg 1. \tag{23}$$

The other notable special case is that the average impedance of the dynamic medium is the same as the impedance of the

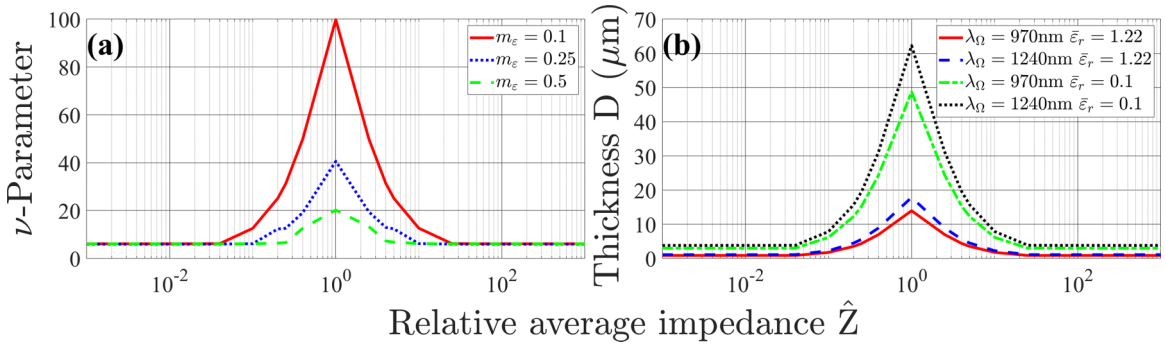

FIG. 4. (a) The first eigenvalue of ν as function of the relative impedance $\hat{Z}$ for three values of the modulation strength m_ε. (b) Here, four different combinations of the average relative permittivity $\bar{\varepsilon}_r$ and the modulation wavelength $\lambda_\Omega = 2\pi c/\Omega$ are used in Eq. (12) with $m_\varepsilon = 0.1$. The slab thickness D corresponding to the smallest ν is graphed as a function of $\hat{Z}$. Here, $\hat{\omega} = 0.5$ and $\varepsilon_r'' = 0.0001$. Note the symmetry about the value $\hat{Z} = 1$. The symmetry for the resonances for $\hat{Z}$ is opposite to those for $1/\hat{Z}$. In the case $\hat{Z} = 1$ there are both symmetric and antisymmetric resonances.

bounding media, namely, $\hat{Z} = 1$. Then, according to Eqs. (21), (17), and Eq. (20) of Ref. [14]

$$\frac{D}{\lambda_\Omega/2} = \left\{ \begin{matrix} (\pi/2)s/m_\varepsilon \text{ for square modulation} \\ 2s/m_\varepsilon \text{ for harmonic modulation} \end{matrix} \right\} \quad \text{for } \hat{Z} = 1. \tag{24}$$

This describes singlets whose half-wavelength fits in the slab width on the order of $(1/m_\varepsilon)$ times, this being a large and not necessarily integer number [as was the case for the doublets in Eq. (22)]. Then we can see that, just as for $\hat{Z} \ll 1$ (or $\hat{Z} \gg 1$), the behavior of the resonances for harmonic modulation differs from the square modulation only by the replacement $m_\varepsilon/\pi \to m_\varepsilon/4$.

In the following section we will compare approximate solutions obtained from Eq. (14) with exact numerical solutions.

III. NUMERICAL RESULTS AND DISCUSSION

To solve Eqs. (3) and (12) a minimum number of harmonics n must be used. For harmonic modulation 30 to 40 harmonics are sufficient while for square modulation at least 50 harmonics are necessary. The following results were obtained using 100 harmonics and 100 p bands for both modulations.

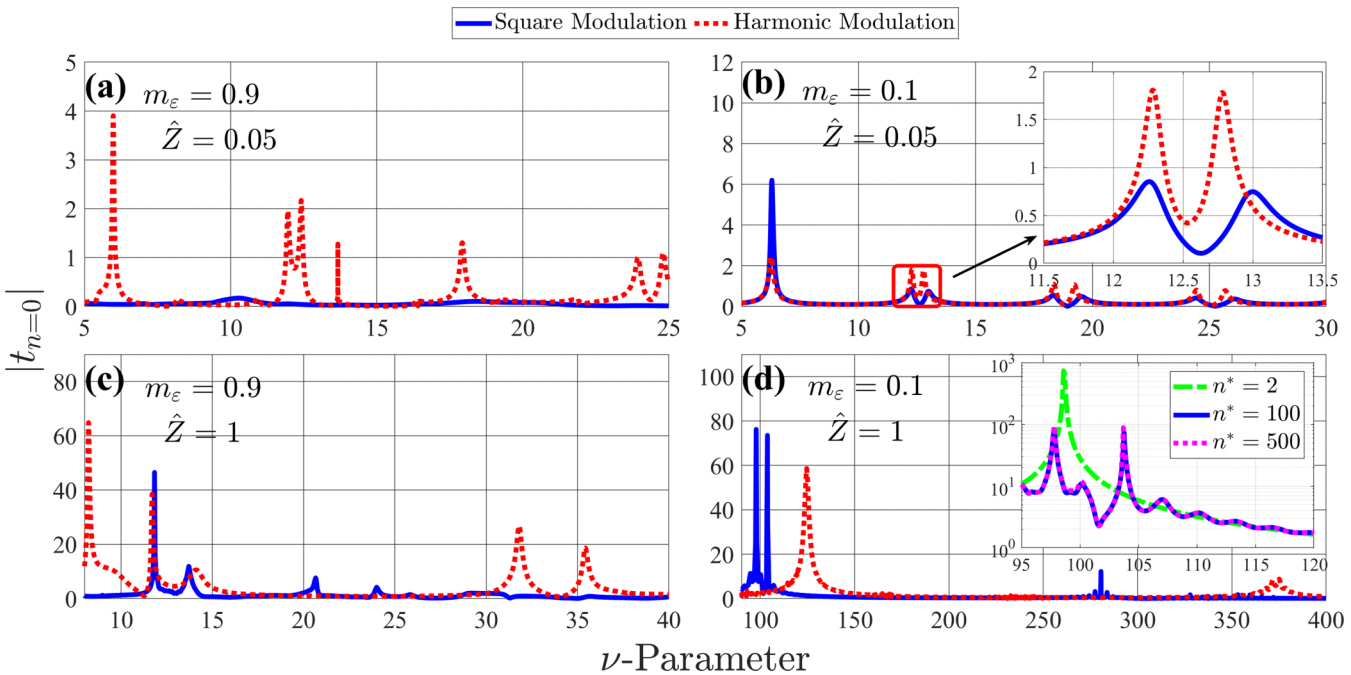

FIG. 5. Magnitude of the transmission coefficient $t_{n=0}$ as function of the ν parameter for (a) $m_\varepsilon = 0.9$ and $\hat{Z} = 0.05$, (b) $m_\varepsilon = 0.1$ and $\hat{Z} = 0.05$, (c) $m_\varepsilon = 0.9$ and $\hat{Z} = 1$, and (d) $m_\varepsilon = 0.1$ and $\hat{Z} = 1$. Results for the square modulation (solid blue lines) are compared with those for harmonic modulation (dotted red lines). Here, $\hat{\omega} = 0.5$ and $\varepsilon_r'' = 0.01$. When $\hat{Z} = 0.05$ there are both symmetric and antisymmetric resonances. The inset of (b) amplifies the doublet at $\nu = 4\pi$. The inset of (d) zooms in on the doublet resonance for square modulation at $\nu = \pi^2/m_\varepsilon \approx 100$. Here, n^* denotes the number of harmonics n.

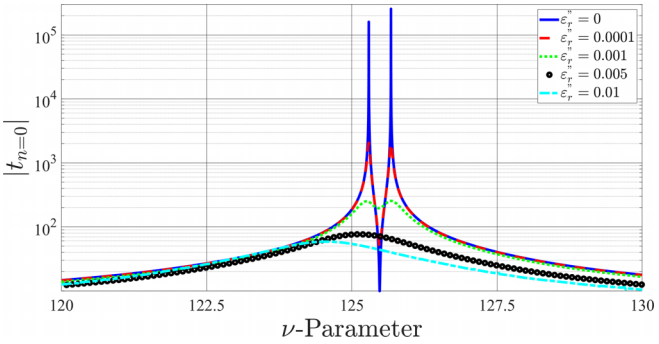

FIG. 6. This figure zooms in at the sharp red peak at $\nu = 4\pi/m_\varepsilon \approx 125$ for harmonic modulation in Fig. 5(d). It shows that, for sufficiently small dissipation ($\varepsilon'' < 0.005$) and with higher resolution, the broad red maximum actually splits into a doublet. Moreover, with $\varepsilon_r'' = 0$, the two sharp peaks keep increasing indefinitely with improved resolution. Same parameters as in Fig. 5(d).

Now we have three methods to calculate the crucial parameter ν, Eq. (9), that specifies the modulation frequencies Ω for which resonances occur for a given slab of width D. Two of these are exact: of these one is based on the maxima of the reflection and/or transmission coefficients r_n and t_n as functions of ν, see Eqs. (10) and (11); the other method solves the eigenvalue equation (12) for ν. The third method is approximate, using Eq. (14), derived for weak modulation, $m_\varepsilon \ll 1$. We compare the results of these methods in Fig. 2(a), plotting three eigenvalues of ν as a function of m_ε, while assuming that $\Omega = 2\omega$ (or $\hat{\omega} = 0.5$) and that $\hat{Z} = 1$. Absorption is neglected, $\varepsilon_r'' = 0$. As can be expected, the results of the two exact methods are invariably indistinguishable. As for the weak modulation approximation, here for $\hat{Z} = 1$ Eq. (14) has been reduced to Eq. (17). It is apparent that ν is inversely proportional to m_ε and that, for a given m_ε, the second and third eigenvalues are, respectively, three and five times greater than the smallest eigenvalue. Moreover, the approximation is excellent up to $m_\varepsilon = 0.25$ and, very good up to $m_\varepsilon = 0.5$, the relative error never exceeding 15%. In Fig. 2(b) we compare three eigenvalues of the ν parameter for square and harmonic modulations, using the two exact methods. The results obtained show that the value of ν is always lower for the case of square modulation regardless of the value of m_ε. For $m_\varepsilon \ll 1$ this displacement is given by the factor $4/\pi \cong 1.27$, as explained by the comments following Eq. (17). This suggests a smaller slab width in the case of square modulation. A closer investigation, based on higher resolution, reveals that the eigenvalues in Figs. 2(a) and 2(b) have a fine-structure. Namely, each solution in these figures is actually composed of two eigenvalues, suggesting a doublet structure. This splitting is displayed explicitly in Fig. 2(c) for both square and harmonic modulations for $m_\varepsilon = 0.1$ and $m_\varepsilon = 0.4$. As can be seen, the splittings are substantially greater for the square modulation. Moreover, we find that the smaller-valued component of the doublet corresponds to an antisymmetric field $[E(-x) = -E(x)]$ in the slab, while the larger-valued component pertains to the symmetric solution $[E(-x) = E(x)]$ with respect to the slab center.

In Fig. 3 we graph the product νm_ε as function of m_ε for five values of the impedance parameter $\hat{Z}$. If $\hat{Z} = 1$, the lowest resonance gives, surprisingly, $\nu m_\varepsilon = \pi^2$ even for $m_\varepsilon = 0.5$, although Eq. (17) has been derived for weak modulation. Now, in Ref. [6] it was found that the results remain unaltered when the parameter $\hat{Z}$ is replaced by its reciprocal, $1/\hat{Z}$. We confirm this in Fig. 3 for the mutually reciprocal values $\hat{Z} = 0.005$ and 200 and for $\hat{Z} = 0.25$ and 4. We also note that, according to Eq. (14), switching between $\hat{Z}$ and $1/\hat{Z}$ interchanges as well symmetric and antisymmetric solutions. Also, with higher resolution, every point in Fig. 3 splits into a symmetric and an antisymmetric ν component.

Fiure 3 suggests that, for any modulation, the ν parameter reaches its maximum value when $\hat{Z} = 1$, namely, when the average impedance of the slab is continuous across its boundaries. This is explicitly confirmed in Fig. 4(a) for three values of m_ε. Considering the definition of ν, Eq. (9), this also corresponds to a maximum of the slab thickness for select values of the average permittivity and of the modulation wavelength $\lambda_\Omega = 2\pi c/\Omega$; this can be seen in Fig. 4(b). We note that these are realistic values taken from an experimental work [8], resulting in thicknesses on the order of tens of micrometers. Thus, the larger the impedance contrast with the bounding medium, the smaller are the slab thicknesses for which resonance is attainable (given $\hat{\omega}$) and, vice versa, if the thickness D is specified, the smaller is the modulation frequency that gives rise to a resonance. The symmetry about $\hat{Z} = 1$ confirms that $\nu(\hat{Z}) = \nu(1/\hat{Z})$.

In principle, a straightforward method to observe these resonances would be measurements of the reflection or transmission coefficients as function of the modulation frequency. The case of harmonic modulation was already investigated in Ref. [14]; in the three following figures we will dwell on both similarities and differences that are present for the square modulation. In Fig. 5 we plot the magnitude of the transmission coefficient t_0 as function of ν, which, according to Eq. (9), is proportional to Ω for a given slab thickness. Four combinations of the modulation m_ε and relative impedance $\hat{Z}$ are given. In each case, several resonances are displayed and, for the same parameter values, compared with the case of harmonic modulation. For both cases of modulation, the transmission coefficients are greatest for $\hat{Z} = 1$ and for relatively small values of ν (that is, Ω or D). We wish to stress, however, that apart from these similarities, the two forms of modulation lead, in general, to qualitatively different responses. For example, especially striking are the sharp resonances for harmonic modulation in Fig. 5(a), totally absent (at least in the present resolution) for the square modulation. Similarly, Fig. 5(c) reveals qualitative differences between the two types of modulations. Thus, the Figs. 5(a) and 5(c) suggest that similarities in behavior found for weak modulation ($m_\varepsilon = 0.1$) are absent for strong modulation ($m_\varepsilon = 0.9$).

The choice of $m_\varepsilon = 0.1$ in Figs. 5(b) and 5(d) invites comparisons with the predictions of Sec. II E that was dedicated to the case of weak modulation, $m_\varepsilon \ll 1$. First consider Fig. 5(b), with the relative impedance $\hat{Z} = 0.005$. The transmission coefficients display a series of doublets, all positioned at the same ν values for both the square and the harmonic modulations. Moreover, these doublets are centered at $\nu = 2\pi$, 4π, 6π, and so on, just as specified by Eqs. (19) and (20). The split (peak separation) is about twice, thrice, and

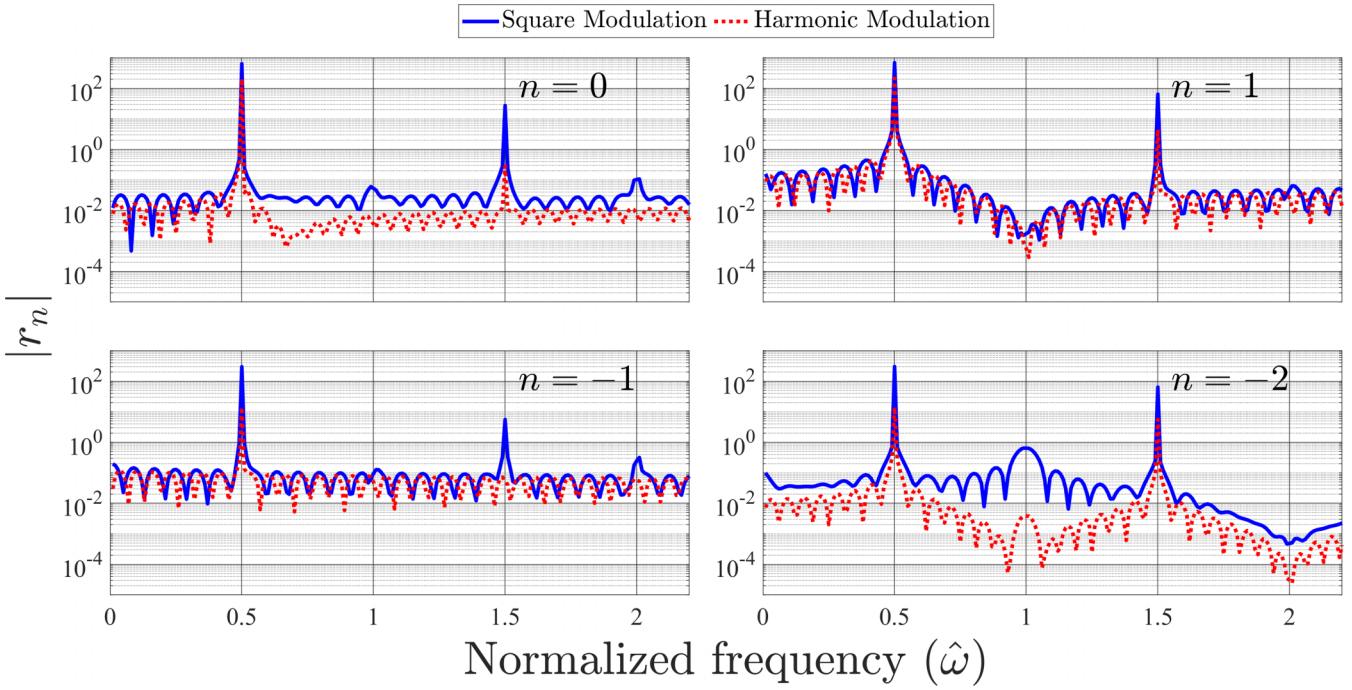

FIG. 7. The magnitude of the reflection coefficients r_n as function of the normalized frequency ω/Ω for four values of the harmonic index n. The first resonance for square modulation ($\nu = 41.0176$, solid blue line) is compared with the first resonance for harmonic modulation ($\nu = 50.2854$, dotted red lines). Here, $\hat{Z} = 1$, $m_\varepsilon = 0.25$, and $\varepsilon_r'' = 0.001$. Note parametric resonances for odd integer multiples of $\Omega/2$ in addition to the usual Fabry-Pérot oscillations.

so on greater for the second, third, and so on doublet as it is for the first one, again confirming the Eqs. (19) and (20). Finally, the inset of Fig. 5(b) also confirms that the split for the harmonic modulations is smaller ($0.1\pi s$) than the split for the square modulation ($0.4s$). Thus, we can conclude that our approximation for $m_\varepsilon \ll 1$ and $\hat{Z} \ll 1$ works just fine for $m_\varepsilon = 0.1$ and $\hat{Z} = 0.05$. Similar behavior can be expected for somewhat greater values of m_ε and, indeed, in Fig. 5(a) we can still observe some semblance to Fig. 5(b) for the harmonic modulation (not, however, for the square modulation) even though m_ε is as large as 0.9. That said, the first resonance peak in Fig. 5(b) does not reveal doublets, although, for ε_r'' sufficiently smaller than 0.01, the peak for square modulation does split.

The situation changes dramatically for continuous average impedance $\hat{Z}$ at the slab boundaries, namely, $\hat{Z} = 1$, while still keeping $m_\varepsilon = 0.1$, see Fig. 5(d). For the harmonic modulation (dashed red lines) resonant peaks can be seen at $\nu \approx 125$ and $\nu \approx 375$, corresponding very well to the approximate result of Ref. [14], $\nu = 4\pi s/m_\varepsilon$ for $s = 1$ and $s = 3$. However, with improved resolution and sufficiently small absorption ($\varepsilon'' < 0.005$) the peak at $\nu \approx 125$ splits into two peaks, indicating a shortcoming of the approximation for $m_\varepsilon \ll 1$, see Fig. 6. Notably, these peaks diverge when $\varepsilon_r'' \to 0$, as proper resonances should. As for the square modulation (solid blue lines) there are two sharp resonances at $\nu \approx 100$ and a single resonance at $\nu \approx 280$. These values correspond to $s = 1$ and $s = 3$ of the weak-modulation approximation, Eq. (17). However, according to this equation, there should be only a single peak at $\pi^2/m_\varepsilon \approx 100$! The explanation is given by the inset of Fig. 6(d): Assuming just two harmonics ($n = 2$) (as assumed in the $m_\varepsilon \ll 1$ approximation) there is a single peak, indeed; a greater number of harmonics ($n \geqslant 100$) is, however, required to reveal the splitting. In this inset we can also observe the convergence of Eq. (11) for a sufficiently large number of harmonics $n^* = 100$ and $n^* = 500$, obtaining practically the same results.

As we pointed out in Sec. II E, the approximation based on just two harmonics ($n = 0,\ 1$), is expected to lead to reasonably accurate results for small modulations, $m_\varepsilon \ll 1$. This is to say that the relative permittivity is essentially approximated by $\varepsilon_r(t) = \bar{\varepsilon}_r + \hat{\varepsilon}_1 e^{i\Omega t}$. Now, for our square modulation model, $\hat{\varepsilon}_1 = -2i\bar{\varepsilon}_r m_\varepsilon/\pi$, while, for the harmonic modulation $\hat{\varepsilon}_1 = -i\bar{\varepsilon}_r m_\varepsilon/2$. This suggests that, for sufficiently weak modulation, results for the square modulation can be gotten from results for the harmonic modulation, simply by replacing m_ε by $(4/\pi)m_\varepsilon$. For continuous average impedance, $\hat{Z} = 1$, the resonance parameter ν is inversely proportional to m_ε, see Eq. (17). In this case, then, the ν values for the square modulation are expected to be diminished by the factor $(4/\pi)$ with respect to those for the harmonic modulation. This is beautifully confirmed by the Fig. 2(b) and the Fig. 5(d) as well. On the other hand, for very small ($\hat{Z} \ll 1$) and for very large ($\hat{Z} \gg 1$) contrast, our approximate calculation predicts ν doublets whose positions are independent of m_ε, while whose splittings are proportional to m_ε, see Eq. (19). Again, this behavior is confirmed by the precise calculation in Fig. 5(b), where the only difference between the two types of modulation is an increase, by the factor $(4/\pi)$, in splitting for the square modulation. Unfortunately, as can be expected, the assumption of just two harmonics ($n = 0, 1$) is not as justified for the square modulation as it is for the harmonic modulation, see inset of Fig. 5(d). Moreover, in the vicinity of the resonances the behavior is acutely dependent on absorption, see

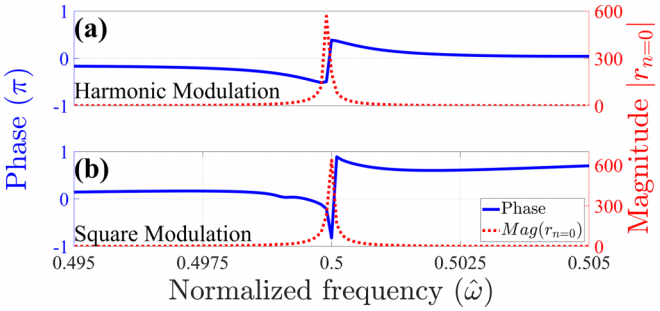

FIG. 8. Phase (solid blue lines, left-hand scale) and magnitude (dotted red lines, right-hand scale) of the reflection coefficient $r_{n=0}$ as function of the reduced frequency $\hat{\omega}$ in the vicinity of $\hat{\omega} = 1/2$. (a) Harmonic modulation, (b) square modulation. Same parameters as in Fig. 7.

Fig. 6. All in all, the $(4/\pi)$ factor for transforming between the two modulations should be exercised with care.

In Figs. 5 and 6 ν was scanned, while the frequency of incidence was fixed at $\omega = \Omega/2$. In Fig. 7, on the contrary, we limit ν to the lowest resonance values for the square modulation ($\nu = 41.0176$, solid blue lines) and the harmonic modulation ($\nu = 50.2854$, dashed red lines). For both profiles of modulation, we plot the magnitude of the reflection coefficient r_n as function of ω/Ω for four values of the harmonic index n. For both square and harmonic modulations, parametric resonances appear at odd multiples of $\Omega/2$ and the usual Fabry-Pérot oscillations are also present. Note that the resonances for square modulation are invariably sharper and higher than for harmonic modulation.

The reflection coefficients exhibit intriguing behavior in the immediate neighborhood of the frequency $\omega = \Omega/2$; in Fig. 8 we zoom in in this region. The magnitude of the reflection coefficient is very large for $\hat{\omega} = 0.5$ and drops to extremely small values outside this frequency. This behavior, not unlike a Dirac delta function, is true for both harmonic modulation, Fig. 8(a), and square modulation, Fig. 8(b). On the other hand, the phase change of the reflection coefficient at $\hat{\omega} = 0.5$ is highly sensitive to the form of modulation, as is manifest by the qualitatively different phase shifts in Figs. 8(a) and 8(b).

IV. CONCLUSION

Much of the recent work on PTCs is concerned with instabilities, namely, growing optical fields excited by wave numbers within bands that are forbidden to monochromatic incidence of light; see, for example, Refs. [8–10]. On the other hand, in the present paper (and in Refs. [13,14] as well) we discussed stable amplification of monochromatic light incident at a PTC slab. Clearly, the extra energy in the reflected and transmitted frequency combs is drawn from the (unspecified) source of modulation of the permittivity $\varepsilon(t)$ of the slab. Here, we compared the behavior of PRs for square and harmonic profiles of $\varepsilon(t)$, pointing out striking differences, as well as similarities, in the reflection and transmission coefficients. For sufficiently weak modulation, $m_\varepsilon \ll 1$, results for the square modulation can be obtained from those for the harmonic modulation by the simple replacement of m_ε by $(4/\pi)m_\varepsilon$. These resonances could be realized in the infrared region for PTC slabs of thickness on the order of tens of micrometers with modest modulation strengths $m_\varepsilon \sim 0.1$. Several topics, associated with PRs would be of interest to explore: duty cycle different than 50%; excitation by oblique incidence; and periodic modulation of $\mathrm{Im}\{\varepsilon_r(t)\}$ [as well as $\mathrm{Re}\{\varepsilon_r(t)\}$]. Moreover, we are also investigating PRs in transmission lines with modulated capacitors (varactors) in the microwave regime. The ideas on PRs commented in this work have the potential to find applications in energy management.

ACKNOWLEDGMENTS

J.L.V.-G. thanks CONACyT for the national scholarship granted during his doctoral studies and P.H. acknowledges CONACyT Grant No. A1-S-45628. J.L.V.-G. greatly appreciates numerous illuminating conversations with J. G. Gaxiola-Luna, as well as for making available to him computer programs for solving certain equations in this paper.

[1] K. Sacha, *Time Crystals* (Springer, New York, 2020).
[2] E. Galiffi, R. Tirole, S. Yin, H. Li, S. Vezzoli, P. A. Huidobro, M. G. Silveirinha, R. Sapienza, A. Alù, and J. B. Pendry, Photonics of time-varying media, Adv. Photon. **4**, 014002 (2022).
[3] R. K. D. M. Solís and N. Engheta, Time-varying materials in the presence of dispersion: plane-wave propagation in a lorentzian medium with temporal discontinuity, Photon. Res. **9**, 1842 (2021).
[4] J. Li, Y. Li, P.-C. Cao, M. Qi, X. Zheng, Y.-G. Peng, B. Li, X.-F. Zhu, A. Alù, H. Chen, and C.-W. Qiu, Reciprocity of thermal diffusion in time-modulated systems, Nat. Commun. **13**, 167 (2022).
[5] R. Yu and S. Fan, Manipulating coherence of near-field thermal radiation in time-modulated systems, Phys. Rev. Lett. **130**, 096902 (2023).
[6] D. Holberg and K. Kunz, Parametric properties of fields in a slab of time-varying permittivity, IEEE Trans. Antennas Propag. **14**, 183 (1966).
[7] J. R. Zurita-Sánchez, P. Halevi, and J. C. Cervantes-González, Reflection and transmission of a wave incident on a slab with a time-periodic dielectric function $\varepsilon(t)$, Phys. Rev. A **79**, 053821 (2009).
[8] S. Vezzoli, V. Bruno, C. DeVault, T. Roger, V. M. Shalaev, A. Boltasseva, M. Ferrera, M. Clerici, A. Dubietis, and D. Faccio, Optical time reversal from time-dependent epsilon-near-zero media, Phys. Rev. Lett. **120**, 043902 (2018).
[9] M. Lyubarov, Y. Lumer, A. Dikopoltsev, E. Lustig, Y. Sharabi, and M. Segev, Amplified emission and lasing in photonic time crystals, Science **377**, 425 (2022).
[10] A. Dikopoltsev, Y. Sharabi, M. Lyubarov, Y. Lumer, S. Tsesses, E. Lustig, I. Kaminer, and M. Segev, Light emission by free electrons in photonic time-crystals, Proc. Natl. Acad. Sci. USA **119**, e2119705119 (2022).
[11] J. R. Reyes-Ayona and P. Halevi, Electromagnetic wave propagation in an externally modulated low-pass transmission line, IEEE Trans. Microw. Theory Tech. **64**, 3449 (2016).

[12] J. R. Reyes-Ayona and P. Halevi, Observation of genuine wave vector (κ or β) gap in a dynamic transmission line and temporal photonic crystals, Appl. Phys. Lett. **107**, 074101 (2015).

[13] J. R. Zurita-Sánchez and P. Halevi, Resonances in the optical response of a slab with time-periodic dielectric function $\varepsilon(t)$, Phys. Rev. A **81**, 053834 (2010).

[14] J. S. Martínez-Romero and P. Halevi, Parametric resonances in a temporal photonic crystal slab, Phys. Rev. A **98**, 053852 (2018).

[15] W. Magnus and S. Winkler, *Hill's Equation* (John Wiley & Sons, New York, 1966).

[16] M. Salehi, M. Memarian, and K. Mehrany, Parametric amplification and instability in time-periodic dielectric slabs, Opt. Express **31**, 2911 (2023).

[17] V. Asadchy, A. G. Lamprianidis, G. Ptitcyn, M. Albooyeh, Rituraj, T. Karamanos, R. Alaee, S. A. Tretyakov, C. Rockstuhl, and S. Fan, Parametric mie resonances and directional amplification in time-modulated scatterers, Phys. Rev. Appl. **18**, 054065 (2022).

[18] J. G. Gaxiola-Luna and P. Halevi, Temporal photonic (time) crystal with a square profile of both permittivity $\varepsilon(t)$ and permeability $\mu(t)$, Phys. Rev. B **103**, 144306 (2021).

[19] J. G. Gaxiola-Luna and P. Halevi, Growing fields in a temporal photonic (time) crystal with a square profile of the permittivity $\varepsilon(t)$, Appl. Phys. Lett. **122**, 011702 (2023).

[20] J. S. Martínez-Romero, O. M. Becerra-Fuentes, and P. Halevi, Temporal photonic crystals with modulations of both permittivity and permeability, Phys. Rev. A **93**, 063813 (2016).